A numerical study on localized volume reduction in elastic media: Some insights on the mechanics of anticracks

R. Katsman,[1] E. Aharonov,[1] and H. Scher[1]

Received 29 December 2004; revised 23 August 2005; accepted 7 December 2005; published 30 March 2006.

[1] Porous rocks, subjected to compressive stress, often undergo mechanical compaction via grain crushing and grain rearrangement, and chemical compaction by pressure solution. Such volume reduction processes are known to spontaneously localize under certain conditions, creating compaction and compacting shear bands, solution seams, and stylolites. However, the localization process is poorly understood. The formation and propagation of compaction bands have recently been studied using an elastoplastic spring network model (Katsman et al., 2005). In this paper, the same technique was employed to systematically analyze localized volume reduction (LVR) defects and their interactions with the surrounding elastic media, i.e., the stress distribution around an LVR region. Simulation results show that LVR regions experience stress concentrations at their tips, reminiscent of mode I cracks. However, aside from this similarity point, comparison of stress around LVR regions to stress around cracks reveals that the stress/strain distribution in such LVR defects is quite different than that surrounding mode I cracks. Implications for stylolites and compaction band are thoroughly discussed.

Citation: Katsman, R., E. Aharonov, and H. Scher (2006), A numerical study on localized volume reduction in elastic media: Some insights on the mechanics of anticracks, *J. Geophys. Res.*, *111*, B03204, doi:10.1029/2004JB003607.

1. Introduction

[2] Porous rocks, as they evolve in the Earth's crust, experience both lithostatic and tectonic compressive stresses. These stresses cause reversible and irreversible volume changes in the bulk and pore volume of rocks. Reversible volume reduction (i.e., elastic strain) in porous rocks describes the elastic closing of cracks and pores, and is reversed upon removal of stress. Irreversible volume reduction in porous rocks occurs by mechanical and chemical compaction, which is retained even upon removal of load (i.e., plastic strain).

[3] Mechanical compaction refers to grain crushing, rearrangement, and subsequent porosity reduction [e.g., *Ramm*, 1992; *Mollema and Antonellini*, 1996; *Bjorkum et al.*, 1998; *Issen and Rudnicki*, 2000, 2001; *Revil et al.*, 2002]. The term chemical compaction is used here to describe pressure solution [e.g., *Paterson*, 1973; *Rutter*, 1976; *Weyl*, 1959], a process by which solid mass is dissolved under high stress, and precipitated in regions of low stress. Pressure solution is the main process by which ductile deformation of the upper crust occurs. It plays an important role in sedimentary basin evolution, in the healing of faults, and in the earthquake cycle. In addition to diffuse and distributed compaction [e.g., *Angevine and Turcotte*, 1983; *Rutter*, 1976; *Ramm*, 1992; *Lehner*, 1995; *Renard et al.*, 1999; *He et al.*, 2002; *Niemeijer et al.*, 2002; *de Meer and Spiers*, 1999], both mechanical and chemical compaction may localize spontaneously.

[4] Mechanical compaction localization features appear as compaction and shear-enhanced compaction bands [*Mollema and Antonellini*, 1996; *Rudnicki and Olsson*, 1998; *Issen and Rudnicki*, 2000, 2001; *Wong et al.*, 1997, 2001; *Baud et al.*, 2004] (Figure 1a). Chemical compaction localization is manifested as elongated solution seams and stylolites, along which pressure solution is highly enhanced. Stylolites appear abundantly in carbonate and other sedimentary rocks [e.g., *Alvarez et al.*, 1978; *Renard et al.*, 2004; *Karcz and Scholz*, 2003] (Figure 1b), and may be responsible for up to 50% volume loss in some rocks [*Stockdale*, 1922; *Alvarez et al.*, 1978; *Ramos*, 2000]. Mechanical and chemical localization features greatly influence fluid storage and transport potential in porous rocks [*Bjorkum et al.*, 1998; *Vajdova et al.*, 2004], thus playing an important role in the management and extraction of oil and gas in the crust [*David et al.*, 2001; *Budd*, 2001, 2002; *Haimson*, 2001, 2003; *Klaetsch and Haimson*, 2002; *Haimson and Kovachich*, 2003]. In addition, these features also influence the elastic properties and the stress and strain distribution in the sedimentary formations in which they appear.

[5] The importance of understanding localization processes prompted a considerable effort [e.g., *Fletcher and Pollard*, 1981; *Fueten and Robin*, 1992; *Dewers and Ortoleva*, 1990; *Koehn et al.*, 2003; *Renard et al.*, 1997, 2004; *Gal et al.*, 1998]. Yet, despite these works, a large disparity still exists between the understanding of reversible and irreversible volume reduction features. Reversible localization of deformation under extension, namely, mode

[1]Weizmann Institute of Science, Rehovot, Israel.

0148-0227/06/2004JB003607$09.00

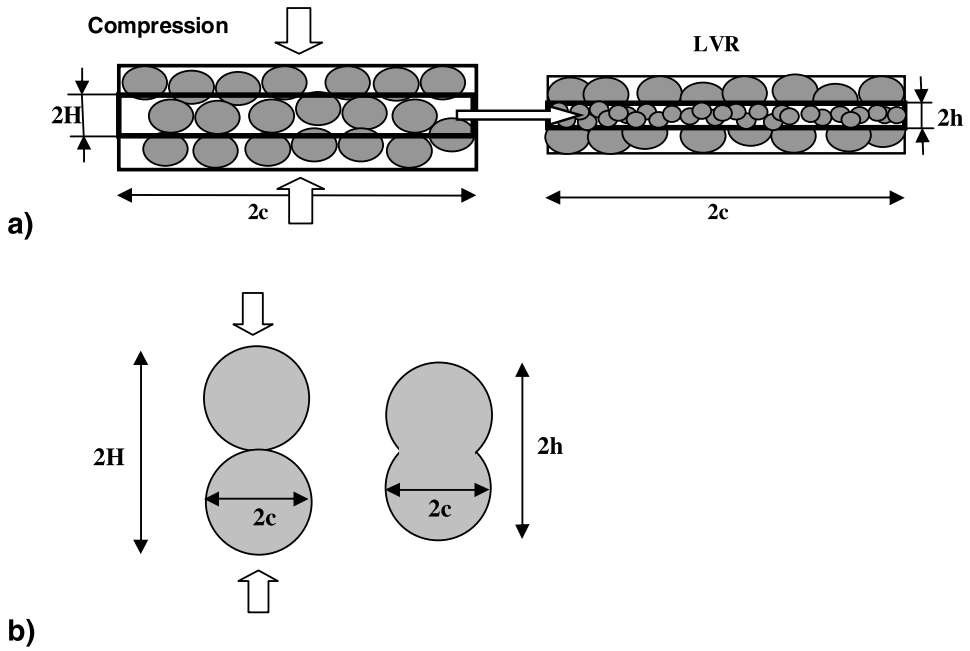

Figure 1. Localized volume reduction, characterized by vertical dimension shortening (2H, before LVR, and 2h, after LVR), and no lateral dimensional changes (2c, before and after LVR) in (a) compaction band in a high-porosity rock and (b) pressure solution on the contact between two grains.

I (opening) cracks, has been quantitatively studied since *Griffith* [1920] (see *Lawn and Wilshaw* [1975] for review). Alternatively, the evolution of irreversible localized volume reduction (LVR) features, their spacing and localization conditions remain largely unexplained.

[6] Mechanistic analysis of localized volume reduction started with the pioneering work of *Fletcher and Pollard* [1981]. They suggested that when a region experiences pressure solution, a stress concentration occurs at the tips of the dissolved region. Since regions of high compressive stress experience enhanced pressure solution, *Fletcher and Pollard* [1981] predict further propagation of planar dissolution zones (i.e., stylolites) in the direction perpendicular to the maximum compressive stress, reminiscent of propagation of mode I cracks. *Fletcher and Pollard* [1981] hypothesized that the observed morphological similarity between cracks and stylolites occurs because the stress distribution surrounding a stylolite is similar to that surrounding a mode I (opening) crack, but with opposite sign. As a result, they suggested that stylolites are "anticracks." The anticrack concept has subsequently been widely invoked in the literature to also explain the formation of compaction bands and deep earthquakes [*Wong et al.*, 2001; *Fueten and Robin*, 1992; *Green et al.*, 1992; *Riggs and Green*, 2005], even though it has never been tested by calculations.

[7] Early quantitative works demonstrated that interactions between stress and dissolution may lead to pressure solution localization [e.g., *Dewers and Ortoleva*, 1990; *Fueten and Robin*, 1992] but did not study the full two-dimensional (2-D) problem of volume reduction localization and its interaction with the stress field in an elastic media. Recently, *Katsman et al.* [2005] addressed the 2-D interaction problem, by modeling mechanical compaction localization and evolution using an elastoplastic spring network model (SNM). In that work it was shown that regions that lost volume via mechanical compaction create a stress concentration at their tip and induce further volume reduction and compaction band propagation. However, detailed stress analysis of LVR features was not performed and is now presented here.

[8] The numerical study presented in this paper explores the stress perturbation induced by a single volume reduction feature in a 2-D elastic media, and the parameters controlling the stress distribution. LVR features are constructed by removal of a thin lamina of matter, followed by closure of the resulting missing space under differential macroscopic compression. Stress distributions within and around LVR features are computed using an elastoplastic version of the SNM [*Katsman et al.*, 2005; *Katsman and Aharonov*, 2006] and are compared to distributions around two other defects in elastic matter: opening and closing mode I cracks, under remote extension and remote compression, respectively. This study focuses on static, nonpropagating, LVR features (an initial study of propagation and evolution of LVR features was presented by *Katsman et al.* [2005]). The stress distribution obtained for the LVR defect differs in an essential way from the main hypothesis of an anticrack in the *Fletcher and Pollard* [1981] model. Our results are interpreted in the context of localization and evolution of volume reduction defects in general, and specifically in their implications for stylolite and compaction band growth.

2. Spring Network Model

[9] For the purpose of studying volume reduction as a problem in an elastic medium with defects, a SNM is

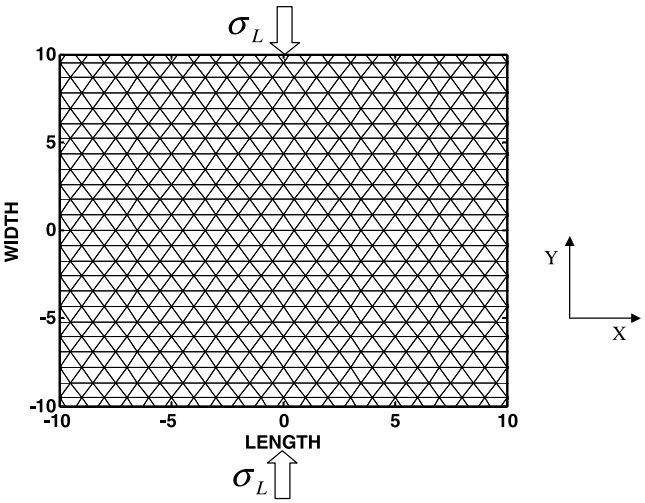

Figure 2. Elastic material is represented as a two-dimensional lattice of nodes connected in a regular triangular array with no topological disorder. The nodes are linked by elastic Hookian springs, macroscopic strain ε_L is applied to horizontal boundaries, and macroscopic stress σ_L is calculated.

utilized (Figure 2). Because of its ability to model highly heterogeneous features and sharp discontinuities in material properties, this kind of model has been used extensively to investigate crack propagation and interaction [e.g., *Curtin and Scher*, 1990a, 1990b; *Schlangen and Garboczi*, 1996, 1997] and was adopted to model compaction, as by *Katsman et al.* [2005] and *Katsman and Aharonov* [2006]. In contrast to a finite element method (FEM) numerical treatment of continuous partial differential equations, the SNM easily allows for a discrete distribution of material properties at a physically relevant scale (microscopic or macroscopic), and also permits natural inclusion of disorder to model heterogeneous media. However, with the SNM, the transfer of stresses from a failed material region to another can only be modeled on the length scale of the spring or larger. A brief description of the model is given below. For a more detailed description of the model and a new algorithm developed to treat compaction, see *Katsman et al.* [2005].

[10] Under the plane strain loading conditions utilized in the model, the three-dimensional equations of elasticity can be reduced to a two-dimensional form, with the 2-D elastic coefficients derived from those in three dimensions, as described by *Thorpe and Jasiuk* [1992]. A two-dimensional elastic material is represented as a lattice of nodes connected in a regular triangular array with no topological disorder (Figure 2). The nodes are linked by elastic Hookian springs with a Young's modulus (E), cross-sectional area (A), and an equilibrium length in a relaxed position (l^{eq}). These variables are put into dimensionless form and set equal to unity; no disorder in material properties is incorporated. The force on a spring connecting nodes i–j, indicating its elastic expansion or contraction, is measured by its length departure from its equilibrium length according to:

$$F_{ij} = F_{ji} = \alpha_{ij}(l - l^{eq})_{ij}, \qquad \alpha_{ij} = \frac{E_{ij}A_{ij}}{l^{eq}_{ij}}, \tag{1}$$

where l is the actual length of the spring, and a positive (negative) force corresponds to an expanded (contracted) spring. To avoid the lattice artifacts mentioned by *Curtin*

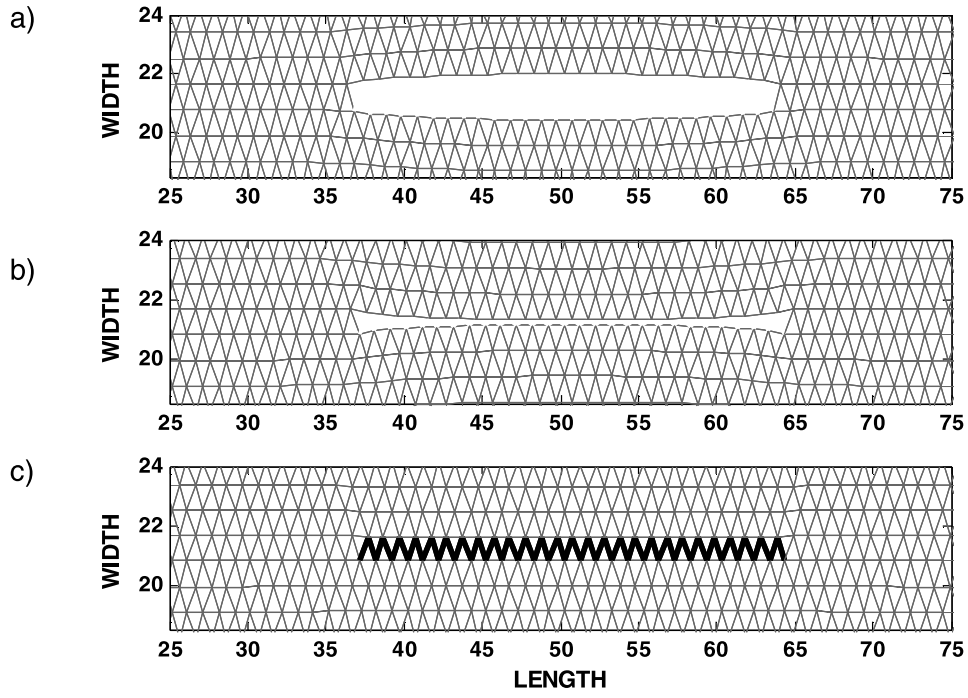

Figure 3. Three defects studied: (a) mode I opening crack under applied extension; (b) mode I closing crack under applied compression; and (c) local volume reduction defect (LVR) under applied compression.

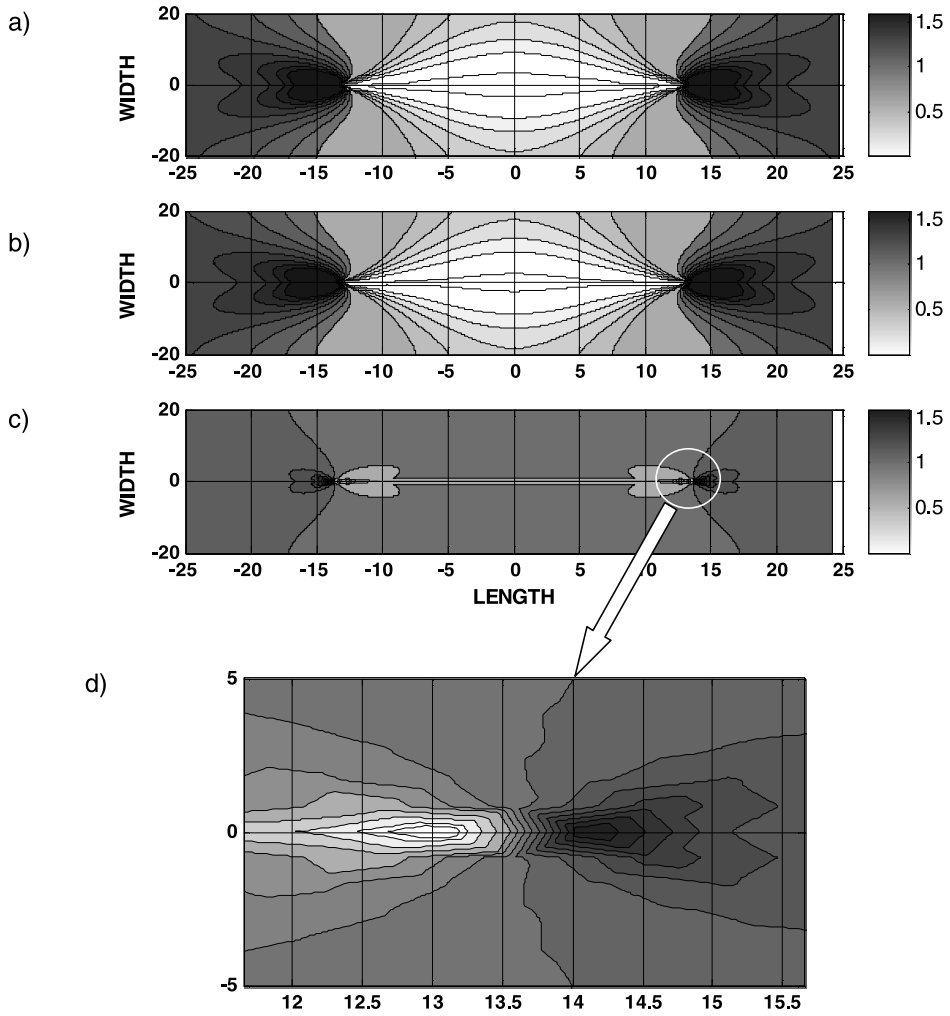

Figure 4. The σ_{yy} stress contours, scaled by the macroscopic remote stress σ_L, around (a) an opening crack; (b) a closing crack; and (c) a local volume reduction defect. The local stress distribution around the crack is identical for both cases of extensive (Figure 4a) and compressive (Figure 4b) loads. Alternatively, the stress distribution around the LVR defect (Figure 4c) is different. (d) Zoom into the LVR defect tip area.

and Scher [1990a, 1990b], caused by using springs as the basic unit, a symmetric triangular unit of springs is considered here as the basic unit for calculations. Therefore the σ_{yy} stress component of the 2-D stress tensor (see Figure 2 for axis orientation) in each unit, due to macroscopic extension/compression, is calculated as the sum of σ_{yy} in the two nonhorizontal springs.

[11] Constant strain rate loading, ε_L, is applied in the Y direction to the horizontal boundaries (see Figure 2) and modeled by a quasi-static sequence of steps. Simulations start from a completely relaxed equilibrium position of the lattice, when displacements of the external boundaries are equal to zero and forces in each spring measured by (1) are zero as well. Then, the external boundary conditions are applied to the nodes at the bottom and top surfaces by moving them to a desired macroscopic strain in the Y direction. In this set of simulations, the top and bottom surface nodes are unconstrained in the X direction, and the side boundaries remain free as well. Maintaining boundary displacement small enough to ensure a linear spring response, the new equilibrium position for each internal and boundary node is found. Calculations are carried out using IML++, the Iterative Methods Library, implemented in C++ by the National Institute of Standards and Technology, USA. Model verification is presented in Appendix A.

3. Modeling Mode I Cracks and LVR Defects

[12] The SNM is commonly used to study mode I cracks propagation and interactions [*Curtin and Scher*, 1990a, 1990b; *Schlangen and Garboczi*, 1996, 1997]. Mode I cracks are modeled by prescribing to springs stress thresholds in extension (F_{ext}^{cr}). If the force on a spring exceeds F_{ext}^{cr}, the spring "breaks" and its Young's modulus is set to zero. "Broken" springs have no resistance to applied stress and effectively simulate bro-

ken matter (Figures 3a and 3b). *Katsman et al.* [2005] suggested a new method to simulate localized volume reduction using the SNM, similarly prescribing permanent changes in spring properties in response to stress. A unit under compression may respond to stress by undergoing compaction, i.e., irreversible volume reduction. Vertical compaction is modeled by removing a thin lamina of material, of thickness $b = 2(H-h)$, from the original height $2H$ (Figures 1a and 1b). Numerically this is done by replacing the nonhorizontal springs equilibrium length l^{eq} (set initially to 1) with a shorter equilibrium length, $l^{eq}_{new} = l^{eq} - \Delta l$, where $\Delta l < 1$. In altered triangular units, the Young's modulus of the horizontal springs is tuned so that although the unit shortened vertically, it retained its original length (as in Figure 3c).

[13] The actual compaction process depends on the underlying physical mechanism. The SNM simulates mechanical compaction as follows: when compressive force on a spring exceeds a critical value F^{cr}_{com}, then the equilibrium length is abruptly shortened to its new value [*Katsman et al.*, 2005]. Pressure solution may be simulated by continuous shortening of springs in response to stress (E. Aharonov and R. Katsman, manuscript in preparation, 2006).

[14] The present investigation consists of two steps: first, a defect with a prescribed size and elastic characteristics is produced; second, the effects on the surrounding stress and the interactions with the surrounding media are investigated. No further defect growth is allowed. To simulate given defects, units belonging to prescribed cracks have a zero stress threshold in extension ($F^{cr}_{ext} = 0$), and those belonging to prescribed LVR defects, are ascribed zero threshold in compression ($F^{cr}_{com} = 0$). To exclude subsequent growth of the defect during the simulations, infinite thresholds in both extension and compression ($F^{cr}_{ext} \rightarrow \infty$, $F^{cr}_{com} \rightarrow \infty$) are prescribed to the rest of the units.

4. Definitions of Cases

[15] This section describes the three types of simulations performed using prescribed defects, each with a given length $2c$. The stress distributions in the vicinity of the defects are reported for a constant macroscopic strain of 0.02 for compression and -0.02 for extension, unless otherwise stated.

[16] Three main patterns are chosen in order to gain insight into the nature of volume reduction and its distinction from other defects:

[17] 1. Mode I (opening) crack is represented by a rectangular void of length $2c$, under crack-normal extension (as in Figure 3a).

[18] 2. Mode I (closing) crack is represented by a rectangular void of length 2c under crack-normal compression (as in Figure 3b). It is important to note that the macroscopic strain is small enough so that the horizontal faces of the crack never touch, and a void is retained throughout the simulations. For both opening and closing cracks (Figures 3a and 3b), the first infinitesimal strain increment is extensive, thus leading to breakage of nonhorizontal springs of the units belonging to the defect (as $F^{cr}_{ext} = 0$).

[19] 3. A local volume reduction defect of length $2c$ under normal compression (as in Figure 3c). At the first infinitesimal compressive increment, the threshold for compression in the prescribed defect is reached (as $F^{cr}_{com} = 0$). Then, a thin lamina of material (of height $b = 2(H-h)$) is removed from the height $2H$ of the units that failed under compression, as described in section 3 (Figure 3c). The resulting single-layer defect is further compressed by increasing remote strain at the horizontal boundary, to simulate removal of material and subsequent complete closing of the hole (as by *Fletcher and Pollard* [1981]). After volume reduction, the physical properties of the material (Young's modulus of nonhorizontal springs) can also be changed in the defect, mimicking natural changes that may occur in the processes accompanied by LVR (e.g., compaction bands may be stiffer than surrounding rock).

5. Results

5.1. Stress Contours

[20] Figure 4 presents contours of the σ_{yy} component of the stress tensor (σ_{yy} is the normal stress acting parallel to the remote compressive stress), scaled to the macroscopic remote stress σ_L, around the defects of the types described above, each with a length $2c \cong 30$.

5.1.1. Opening Crack

[21] It is readily seen that the crack surface is characterized by a zero σ_{yy}/σ_L stress contour, while the maximum stress concentration occurs in peaks outside the crack tips only, as expected from analytical considerations (Figure 4a).

5.1.2. Closing Crack

[22] The local stress distribution around a closing crack is identical to that of an opening crack (Figures 4a and 4b), as is also expected from analytical considerations. Note the opposite sign of σ_L in the two cases. Since closing cracks have shown a stress distribution identical to the one shown by opening cracks, they will not be modeled separately.

5.1.3. Volume Reduction Defect, With Young's Modulus $E = 1$

[23] The stress along the defect is low, as it is for cracks, but as opposed to the crack case, the stress is greater than zero (except at the peak inside the defect tip as seen in Figures 4c and 4d). A maximum and minimum stress concentration around the LVR defect occurs in two opposite peaks outside and inside the defect tips, respectively. It is obvious that the stress distribution around the LVR defect is different from the stress around an opening/closing crack, shown in Figures 4a and 4b.

5.2. Stress Along the Defect

[24] Figure 5 shows σ_{yy} scaled to σ_L, as function of horizontal distance along a mode I crack and LVR defect. Stresses arising from two different defect lengths, $2c \cong 30$ and $2c \cong 50$, are compared in each of the two cases.

5.2.1. Mode I Crack

[25] Along the crack, the stress is zero, as expected. Outside the crack tip, the stress abruptly grows, and then subsides gradually with horizontal distance from the crack (Figure 5a). The tip stress depends strongly on the crack length (*Lawn and Wilshaw* [1975], see also Figure 7a and detailed analysis in section 5.3.1).

5.2.2. Volume Reduction Defect, $E = 1$

[26] Within the defect the stress is nonzero, with a normalized value, σ_M/σ_L, independent of defect length: Figure 5b shows that $\sigma_M/\sigma_L \cong 0.4$ at applied macroscopic

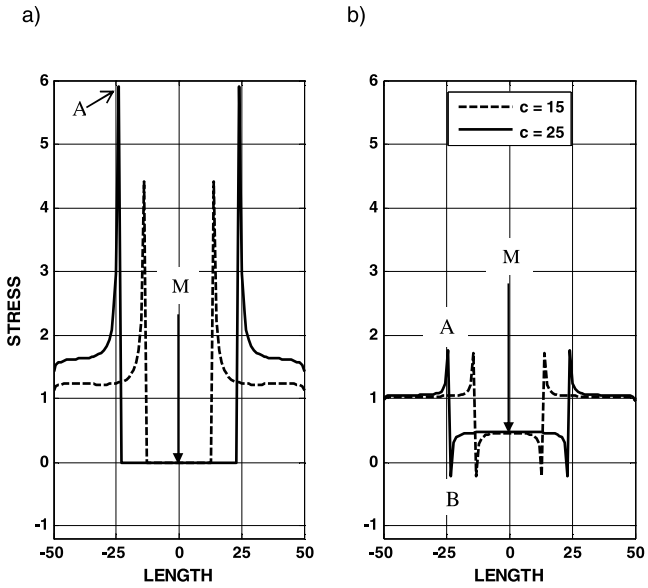

Figure 5. The σ_{yy}/σ_L stress distribution as function of horizontal distance along the defect in (a) a mode I crack and (b) an LVR defect. In Figure 5a, inside the crack (designated by M) the stress is zero. Stress at the tip (designated by A) shows a strong dependence on the crack length. Figure 5b, along the LVR defect (M), the stress is nonzero. In the vicinity of the LVR defect tip, two stress concentration peaks, with opposite trends, are observed (A and B). As opposed to a crack, the stress outside the defect tip (A) is only very weakly dependent on the defect length.

strain $\varepsilon_L = 0.02$ for both $2c \cong 30$ and $2c \cong 50$ (σ_M is σ_{yy} in the middle of the defect, Figure 6). Note that there are two stress peaks in the vicinity of each tip of the defect. The stress at the peak inside the defect tip, σ_B (unit B in Figure 6) is slightly extensive, whereas the stress outside the defect tip, σ_A (unit A in Figure 6), is highly compressive. As opposed to a crack, the normalized stress outside the tip of the LVR defect, σ_A/σ_L, depends only weakly on the defect length. Again, it is readily seen that the stress distribution around the LVR defect is different from that around opening crack.

5.3. Stresses at the Tips of Defects

[27] For a mode I crack, a maximum stress concentration with a strong dependence on crack length, occurs outside the crack tip (Figures 4a and 5a) (see also equation (A4a) in Appendix A). This stress concentration occurs because a crack in an elastic domain represents an area that is unable to support load. As a result, the stresses at the tips of mode I cracks compensate for the load unsupported by the entire length of the crack. Owing to this stress concentration, mode I cracks tend to propagate in the plane, accelerating with increasing crack length.

[28] In contrast to mode I cracks, LVR regions support stresses. The source of the two-peak phenomenon in the LVR region can be understood as follows (Figure 6): Material outside the LVR defect tip (unit A) is compressed by the adjacent defect from which a layer of material was removed and which experienced permanent vertical shortening. Alternatively, the material inside the defect tip (unit B) is pulled at and extended by its surroundings.

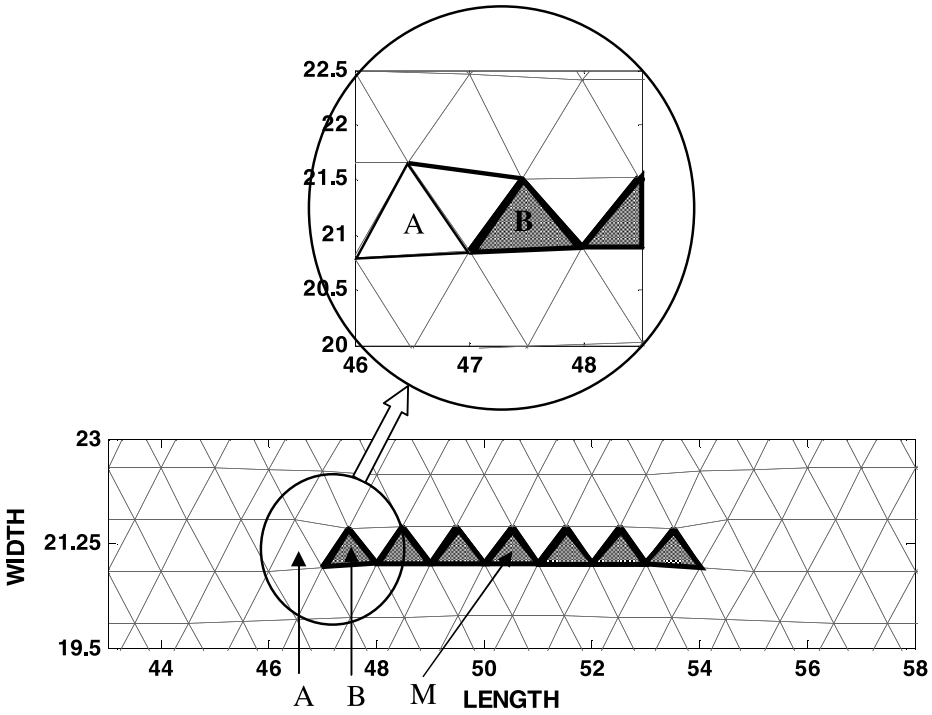

Figure 6. Geometrical incompatibility between undamaged material and LVR defect. Material outside the defect tip (region A) is compressed by the adjacent defect from which a layer of material was removed. At the same time the contracted material inside the defect tip (region B) is pulled at, and extended, by its nondeformed surroundings. The letter M defines the middle of the defect.

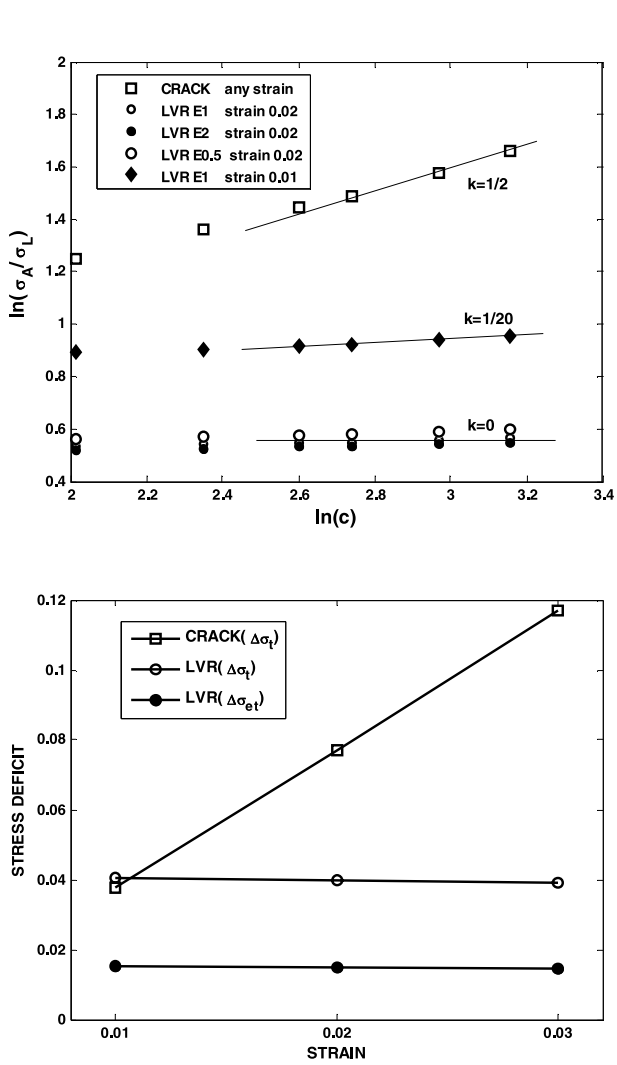

Figure 7. (a) A log-log plot of normalized stress outside the defect tip, σ_A/σ_L, as a function of defect's half length, c. In mode I cracks (top curve), the stress dependence on the defect length is clearly observed. In sharp contrast, for the volume reduction defects at strains 0.01 (middle curve) and 0.02 (three bottom curves presenting results from runs using E_{LVR} = 0.5, 1.0, 2.0), a very weak or no dependence of the stress outside the defect tip on the half length of the defect is detected. Moreover, in contrast to cracks, in LVR defects normalized stress depends on strain. (b) The $\Delta\sigma_t$ and $\Delta\sigma_{et}$ at both crack and LVR tips, as a function of remote strain. For the LVR defect, the stress deficits, $\Delta\sigma_t$ (open circles) and $\Delta\sigma_{et}$ (solid circles), are independent of the macroscopic strain. This again is not expected, nor seen, for cracks, where $\Delta\sigma_t$ (open squares) increases linearly with strain.

The two stress peaks are a result of the missing layer of thickness $b = 2(H-h)$ (Figure 1), removed from the elastic media by the volume reduction process. Removal of volume is equivalent to a permanent strain which persists even under no load. At $\varepsilon_L = 0$, the missing volume will lead to an extensive stress along the defect (e.g., σ_M and σ_B) and a compressive stress σ_A outside the defect tip and around it (see Figure 6). This is in contrast to the stress σ_A outside the crack tip, which appears only under application of external loading ($\varepsilon_L \neq 0$). Therefore it is appropriate to call the strain and stress associated with the LVR defect irreversible, while the ones associated with a mode I crack are called reversible. For more on the subject of stresses due to volume removal, see *Eshelby* [1957] and Appendix B.

5.3.1. Influence of the Length of the Defect

[29] Figure 7a shows normalized stresses, σ_A/σ_L, measured in the peaks outside the crack tip and outside the LVR tip as a function of the defect half length, c. (To account for finite lattice affects, a modification factor, M (equation (A3) in Appendix A), should be included. This has been done for the crack case (following equations (A4a) and (A4b)) but not for the LVR case, as there is no analytical formulation of M for LVR features. However, for large enough lattices, the modification factor is expected to be close to 1 and thus of small influence.) The middle curve presents simulation results for the LVR defect with Young's modulus E_{LVR} = 1.0, under compressive strain ε_L = 0.01. (Here and further, E_{LVR} relates to the Young's modulus of the defect instead of E.) The three coinciding curves in the bottom show results from simulations with LVR defects with Young's modulus of E_{LVR} = 0.5, 1.0, 2.0, correspondingly, under compressive strain ε_L = 0.02.

[30] The upper curve shows results for a mode I opening/closing crack. The tip stress dependence on crack length is clearly observed, and is well fitted by $\sigma_A/\sigma_L \propto c^{1/2}$ (for long enough cracks with $\ln(c) \geq 2.7$), thus convincingly coinciding with Griffith theory (equations (A4a) and (A4b) in Appendix A). This is also the verification for the SNM, as discussed in Appendix A. In sharp contrast, for the volume reduction defects, a very weak or no dependence of σ_A/σ_L on c is observed ($\sigma_A/\sigma_L \propto c^k$, $k \cong 1/20$ when $\varepsilon_L = 0.01$, and $k \cong 0$ when $\varepsilon_L = 0.02$).

5.3.2. Influence of the External Stress

[31] Another feature by which the LVR defect is different from a crack is that for LVR defects the normalized stress in the peak outside the tip, σ_A/σ_L, varies as function of σ_L. Figure 7a shows that σ_A/σ_L resulting from an applied strain ε_L = 0.01, is much greater than that resulting from application of an external strain of ε_L = 0.02. In contrast, it was verified that as long as the crack remains open (its horizontal faces do not touch), the value of the normalized stress in the peak outside the crack tip, σ_A/σ_L, does not depend on the specific macroscopic strain applied. Therefore σ_A/σ_L is invariant, as expected from Griffith theory.

[32] To study stresses produced by LVR defects, it is convenient to define two new variables that describe stress deficits, $\Delta\sigma_t$ and $\Delta\sigma_{et}$. Specifically, $\Delta\sigma_t$ is defined as the difference between σ_{yy} in the peak outside the defect tip (σ_A) and that in the peak inside the defect tip (σ_B): $\Delta\sigma_t = \sigma_A - \sigma_B$. Another stress deficit variable, $\Delta\sigma_{et}$, is defined as the difference between σ_{yy} in the peak outside the defect tip (σ_A) and the remote stress (σ_L): $\Delta\sigma_{et} = \sigma_A - \sigma_L$. Figure 7b shows $\Delta\sigma_t$ and $\Delta\sigma_{et}$ at both crack and LVR tips. For the LVR defect, the stress deficits, $\Delta\sigma_t$ (empty circles) and $\Delta\sigma_{et}$ (full circles), are independent of the macroscopic strain. This again is not expected, nor seen, for cracks, where $\Delta\sigma_t$ (squares) increases linearly with strain.

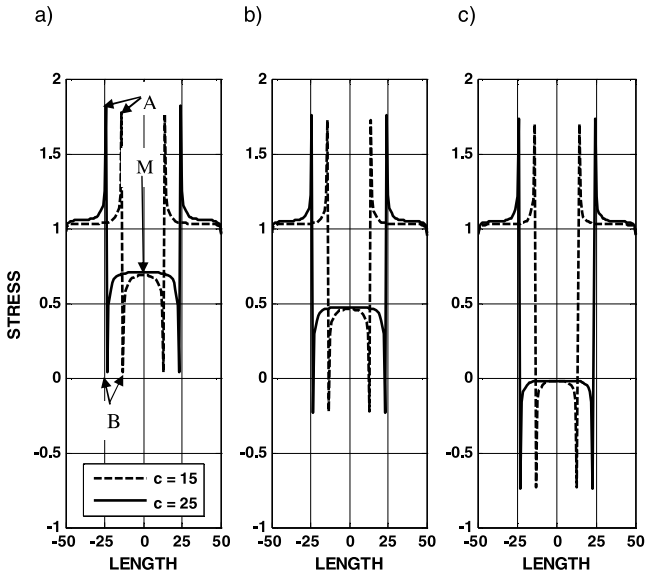

Figure 8. The σ_{yy}/σ_L stress distribution as function of horizontal distance along the LVR with different Young's modules: (a) $E_{LVR} = 0.5$, (b) $E_{LVR} = 1.0$, and (c) $E_{LVR} = 2.0$. Stress inside the tip (point B) and in the middle of the defect (point M), decreases as E_{LVR} grows, whereas the stress stays constant outside the tip (point A).

5.3.3. Influence of the Young's Modulus of the Volume Reduction Defect

[33] The influence of the Young's modulus within the volume reduction defect on the state of stress is an important issue, as the physical processes that affect volume reduction may also affect the Young's modulus. Brittle compaction may be accompanied by hardening, or softening [*Katsman et al.*, 2005; *Katsman and Aharonov*, 2006]. Stylolites and pressure solution may form clay-rich layers, with resulting softening [*Fueten and Robin*, 1992].

[34] To test the effect of the Young's modulus, a new value for the elastic modulus within the transformed defect is prescribed and termed E_{LVR}. (Note that the scenario where E_{LVR} changes within the defect may be more applicable to compaction bands than for stylolites. In compaction bands, a finite region is reduced in volume and transformed in character, while for stylolites, dissolution occurs on an infinitesimally thin layer, changing only its properties, instead of being distributed over a larger rock volume.) The surrounding matrix retains the original Young's modulus, $E = 1$. Normalized stress along the defect is shown in Figure 8 for three different Young's modules in the defect, $E_{LVR} = 0.5$, 1, 2.0 for a, b and c respectively, at external strain $\varepsilon_L = 0.02$. It is seen that the larger the Young's modulus, the smaller the stress is within the defect (point M in Figure 8), and the smaller the stress is at the peak inside the defect tip (σ_B/σ_L calculated at point B). Despite this, the normalized stress σ_A/σ_L at the peak outside the defect tip (point A) remains independent of E_{LVR} of the defect (see three bottom coinciding curves in Figure 7a). As a consequence, as shown in Figure 9a, the stress deficit, $\Delta\sigma_t$ between the stresses inside and outside the LVR defect tip, grows with E_{LVR}.

5.3.4. Influence of the Amount of Removed Material in the Volume Reduction Defect

[35] To test how the stress deficit for LVR defects depends on the amount of removed material, several simulations with different height $b = 2(H-h)$ removed from the LVR defect were performed. This is done by controlling l^{eq}_{new} of nonhorizontal springs within the LVR defect. The relation between b and porosity loss during compaction is discussed by *Katsman and Aharonov* [2006]. The relationship between the thickness of the region removed, b, and $\Delta l = l^{eq}_{old} - l^{eq}_{new}$, the amount of spring shortening, is

$$b = \frac{\sqrt{3}}{2} l^{eq}_{old} - \sqrt{\left(l^{eq}_{old} - \Delta l\right)^2 - \frac{\left(l^{eq}_{old}\right)^2}{4}}.$$

Figure 9b shows that the stress deficit, $\Delta\sigma_t$, depends linearly on b. This result agrees with the concept presented in Figure 6 and suggests that the stress deficit, $\Delta\sigma_t$, originates from the irreversible strain caused by the amount of removed material, b.

6. Discussion

6.1. Source of the Stress Behavior

[36] The stress at the tip of the LVR, and its functional dependences on defect length, removed volume, applied stress, and internal defect modulus E_{LVR}, as observed in Figures 7, 8, and 9, can be heuristically explained as follows. When a volume of vertical extent $b = 2(H-h)$ is removed from a body, the elastic defect can still carry and transmit stress; in this it is different from cracks. The only reason for a stress concentration at the peak outside the tip of this defect, σ_A, is that the missing height b creates a permanent compressive strain, expected to be proportional to b. Moreover, σ_A is also expected to be proportional to the Young's modulus E of the undamaged material [*Eshelby*,

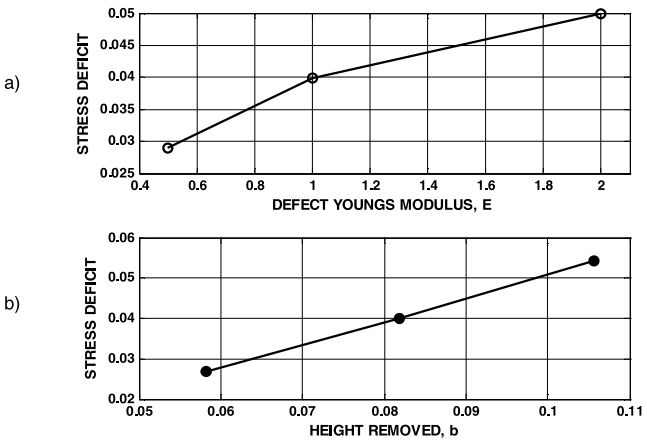

Figure 9. Stress deficit outside the tip of an LVR defect, $\Delta\sigma_t$, as function of (a) Young's modulus E_{LVR} of the defect and (b) the height $b = 2(H - h)$ that was removed in unstrained conditions. (a) Stress deficit outside the tip of an LVR defect $\Delta\sigma_t$ increasing nonlinearly with E_{LVR} (b kept constant); (b) $\Delta\sigma_t$ increasing linearly with b ($E_{LVR} = 1$ kept constant).

1957]. As a result, to a first approximation, this tip stress is expected to follow:

$$\sigma_A \sim bE. \quad (2)$$

Similarly, the stress in the peak inside the defect's tip, σ_B, is expected to be proportional to the Young's modulus of the defect, E_{LVR}:

$$\sigma_B \sim -bE_{\mathrm{LVR}}, \quad (3)$$

As a result,

$$\Delta\sigma_t = \sigma_A - \sigma_B \sim b(aE + dE_{\mathrm{LVR}}). \quad (4)$$

The values of the constants, a and d, should also reflect the fact that the stress response is distributed among several units and not concentrated at the tip of the defect only.

[37] Figures 9a and 9b demonstrate that as expected from equation (4), $\Delta\sigma_t$ increases with both b and E_{LVR}. Moreover, Figures 7, 8, and 9 show that the missing height (b), combined with the Young's modulus of the surrounding matrix (E), determine the stress σ_A outside the tip of the LVR defect, whereas the Young's modulus of the defect (E_{LVR}), combined with b, controls stress inside the tip, σ_B, as predicted by equations 2 and 3. It should be noted that Figure 9a shows a slight nonlinearity in the dependence of $\Delta\sigma_t$ on E_{LVR}, which is not predicted by Equation 4. This slight nonlinearity is probably due to the fact that the coefficient d might be dependent on E_{LVR}.

[38] Moreover, Figures 4 and 5 show that compared to cracks, LVR defects induce in the surrounding media a stress disturbance that is more spatially confined. Since load is supported by the LVR defect, normalized stresses drop rapidly to 1.0 away from the LVR tip, as opposed to a crack where stress unsupported by the broken material induces increased load in a relatively large region surrounding the tip.

6.2. Comparison to Previously Proposed Forms of Anticracks and Natural Features

[39] The term "anticrack" used in the literature [*Fletcher and Pollard*, 1981; *Dundurs and Markenscoff*, 1989] has different interpretations depending on what feature is considered opposite to that of a "crack." In this section, previously proposed forms of anticracks will be reviewed, and the relation between these features and our modeling results will be discussed.

6.2.1. Anticracks Formed by Localized Volume Removal

[40] In their classic paper, *Fletcher and Pollard* [1981] (FP) hypothesized a physical basis for the origin and propagation of localized pressure solution seams and stylolites. It was suggested that discrete solution surfaces originate at stress concentrations and propagate through the rock as "anticracks," i.e., as elastic defects with a stress distribution identical to mode I (opening) cracks but with opposite signs. The pressure solution rate in rocks was assumed to be a function of local compressive normal stress only. To explain the localization of pressure solution in long seams, and the fact that these seams have undergone more dissolution in their middle and appear tapered toward their edges, FP considered a gedanken experiment of pressing the walls of a thin lamina, removed from a two-dimensional elastic sheet, together until perfect contact, to form the solution surface. FP suggested that there exists a lamina geometry such that the stress on the surfaces becomes larger than the remote stress. If such a geometry exists then they further suggest that the stress in the formed defect is identical, but with opposite sign, to that of an opening crack.

[41] The inverted mode 1 crack shape, i.e., displacement with an elliptical profile with maxima in the middle of the lamina, would require interpenetration of the lamina walls into each other. For this to be physically realized FP assume that the interpenetrated matter is continuously dissolved (at the high stress points). In analogy with mode I (opening) cracks, there is also a compressive stress concentration at the tip of the anticrack, which leads to increased dissolution, and sideways propagation of the anticrack, or stylolite. Fletcher and Pollard consider this construct to be a relevant description of localized pressure solution seams.

[42] Our results can now be compared to this hypothesis. When a thin lamina is cut and then compressed (however, the lamina faces are not in contact yet) indeed σ_{yy} and ε_{yy} are exactly opposite to that of an opening crack. Therefore the mode I closing crack, for which the walls have not yet touched, may also be named anticrack. However, when enough remote compression is applied, the crack faces close. In this case, the simulations presented above show that any localized volume removal results in the creation of a low stress σ_M on the flanks of the defect (e.g., see point M in Figures 5 and 8), exactly the opposite from the enhanced stresses on the lamina faces suggested by Fletcher and Pollard. As explained in section 5, σ_M depends on the modulus of the defect (see Figure 8). Recent analytical work [*Katsman et al.*, 2006] shows that σ_M depends also on the amount of volume removed, b. Further, when volume reduction occurs under remote compression (since the lamina faces touch each other), stress is transmitted across the defect, and is therefore supported by it, contrary to that in cracks. The pattern of a LVR defect, obtained after dissolution or removal of a lamina of thickness b, differs considerably from that of a crack.

[43] Since the state of stress surrounding the LVR defect will determine the progressive evolution of the stress-induced physical process, the low stress σ_M, on the LVR walls, which is smaller than the surrounding stress σ_L, ensures that no further normal-stress-induced processes will localize on the LVR walls. The resulting LVR feature will thus not thicken with applied macroscopic strain, and not show a self-similar profile, as cracks and fractures do (i.e., their aperture increases as function of crack length [*Scholz*, 2000]). Stress-driven volume reduction will continue to localize at the edges of the defect, where $\sigma_A \gg \sigma_L$, thus lengthening it, while keeping its width constant. Even this lengthening is different than in cracks. Crack growth is accelerated by the increasing stress concentration at the tip as the crack lengthens. Alternatively, since the stress elevation above the background stress at the LVR tip, $\Delta\sigma_{et}$, remains constant with increasing defect length, accelerated

propagation of LVR defects is not expected. The resulting LVR feature is expected to be long and narrow if the kinetics of volume reduction processes depends on elastic normal stress distribution alone. These conclusions lead to important insights regarding the formation processes of the three features which were previously described in the literature as anticracks: (1) compaction bands, (2) stylolites, and (3) spinel lenses formed by phase transformation from olivine:

[44] 1. Compaction bands (CBs) are formed in initially high-porosity rocks by a localized brittle process of grain crushing and intergranular porosity reduction. CBs are observed to be planar features of localized, compression-induced, volume reduction [*Mollema and Antonellini*, 1996; *Rudnicki and Olsson*, 1998; *Issen and Rudnicki*, 2000, 2001; *Olsson*, 1999, 2001; *Olsson and Holcomb*, 2000; *Wong et al.*, 1997, 2001]. Therefore their propagation was suggested to be well described as anticracks; that is, stress at their tips induces further brittle compaction [*Vajdova and Wong*, 2003; *Vajdova et al.*, 2003]. Indeed, in simulations [*Katsman et al.*, 2005; *Katsman and Aharonov*, 2006], CBs are seen to propagate laterally due to self-induced stress concentrations at their tips. Although driven by stress concentration at their tip as cracks are, CBs appear as long and narrow features, having a constant height and not self-similar shapes. In this feature they agree perfectly with the process of LVR suggested here and by *Katsman et al.* [2005] and *Katsman and Aharonov* [2006]. It is worth noting that CBs are likely associated with LVR having increased Young's modulus $E_{\mathrm{LVR}} > 1.0$ (see Figure 8c).

[45] 2. Stylolites, which are a result of a localized pressure solution process, have never been formed in the lab, neither were they fully modeled in a combined elastic and dissolution model. There is inference from field data [e.g., *Alvarez et al.*, 1978; *Ramos*, 2000; *Stockdale*, 1922] that stylolites undergo continued dissolution along the initial surface, with up to 50% rock mass removed by this dissolution. In unpublished data, sets of dissolution seams were reported to even have self-similar width to length aspect ratios (R. C. Fletcher, personal communication, 2005). However, continued localized dissolution along a previously formed solution seam or stylolite, must occur in an environment of reduced normal stress (Figure 5b). This statement must be true since after some initial dissolution, these features may be described as LVR defects, which have lower stress on their walls than all other regions in their vicinity. This conclusion is strengthened by the results from a study by *Fueten and Robin* [1992], who investigated the propagation of LVR driven by compression. In agreement with our results, they saw that their "anticrack" did only lengthen with time, without thickening or continued dissolution along these seams. However, once it is clear that no further dissolution is expected on the stylolite walls due to vertical stress alone, the question remains as to what process may lead to dissolution of up to 50% of rock mass? The solution to this problem must lie in other driving forces for dissolution offsetting the reduced normal stress. Possibly, further dissolution on stylolite walls is controlled by strain energy due to large tangential stresses [e.g., *Gal et al.*, 1998; *Renard et al.*, 2004]. Another explanation is that vertical stress is indeed the driving force behind initial localized dissolution, but the increasing concentrations of clay or other insoluble minerals in the seam, increases the solubility by a large amount, thus offsetting the lowered vertical stresses on the defect [*Dewers and Ortoleva*, 1990; *Walderhaug and Bjorkum*, 2003; *Renard et al.*, 1997]. The different factors affecting stylolite dissolution are under current theoretical modeling. (However, having brought up this problem, LVR still represents what happens when dissolution is driven by normal stress alone.) Stylolites may be associated with a Young's modulus $E_{\mathrm{LVR}} = 1.0$ (see Figure 8b) or with $E_{\mathrm{LVR}} \ll 1$ due to concentration of weak clays (Figure 8a).

[46] 3. Anticracks have also been used by *Green et al.* [1992] to describe a particular form of instability observed during a set of experiments investigating phase transformation from olivine to spinel attempting to explain the physics of deep earthquakes. The transformation is a volume decreasing exothermic phase transformation, which occurs under high temperatures and pressures. In a narrow temperature and pressure range, instead of a homogeneous transformation, the olivine sample undergoes transformation only in localized lenses of spinel [*Riggs and Green*, 2005]. When these LVR lenses coalesce, the sample fails, by some process analogous to a fracture. The observed spinel lenses are relatively thick, and have been termed by *Green et al.* [1992] anticracks. From modeled stress distributions surrounding LVR defects (Figure 4c), it is suggested that the stresses alone cannot account for the observed lens shape, since they favor planar, and not a lens shape, distribution of nucleation sites. Rather, the lens shape may be caused by radial heat diffusivity from the exothermic reaction. Moreover, our finding that in contrast to cracks, LVR tip stress does not increase with LVR defect size, might affect the evolution of crack-like instabilities, in the olivine-spinel transition.

6.2.2. Anticracks Formed by a Rigid Inclusion

[47] A completely different definition of anticrack used in the field of materials science, was given by *Dundurs and Markenscoff* [1989]. The authors considered an anticrack as a slit crack filled with an infinitely rigid lamella, which unlike a crack transmits tractions, but prevents a displacement discontinuity [see also *Markenscoff*, 1993; *Markenscoff and Paukshto*, 1995; *He*, 1998]. The 3-D analytical solutions of the anticrack alone, and the anticrack combined with cracks, under different modes of loading, were derived by *Chaudhuri* [2003a, 2003b]. This anticrack formulation is unlike the LVR studied here, as no irreversible volume reduction occurs within the defect under the loading. The SNM used in the current manuscript is also able to model such an anticrack under loading, prescribing infinitely large Young's modulus to the springs within the defect, while no irreversible volume reduction occurs during loading. See Appendix B for *Eshelby*'s [1957] take on this problem.

6.2.3. Localized Volume Increase

[48] A further extension of the localized volume reduction (LVR) analysis presented here may be performed to study localized volume increase (LVI) features, such as veins [*Vanucchi*, 2001]. Veins appear due to a combination of a stress regime and a fluid pressure, leading to the occurrence of fracture followed by its subsequent mineralization. Veins will retain an added volume when the external stress is removed, as opposed to cracks, which are com-

pletely reversible and retain no added volume after removal of the external stress. Therefore veins are associated with a transformation similar to *Eshelby* [1957] (see Appendix B), with a volume increase (Figure 1 and B1 where b is negative), instead of the volume decrease that we have been dealing with throughout this paper. As a result, veins induce extension at their tips (opposite to the compression generated outside the tips of LVR defects) even in the absence of remote extension. An important conclusion is that mineralization at faults may affect not only their cohesion, but also the whole stress field surrounding the fault, which may have implications for faults and earthquake stress cycles.

7. Conclusions

[49] The large stresses naturally experienced by buried rocks may cause a process of volume reduction via mechanical and chemical compaction, and via phase transformations. Although volume reduction in rocks plays a major role in determining the rocks' mechanical and transport properties, systematic understanding of the stress field in the elastic media induced by irreversible volume reduction processes, is still very limited. In particular, the observed localization of volume reduction (i.e., compaction bands and stylolites) is still poorly understood.

[50] In order to gain insight into patterns of stress concentrations induced by localized volume reduction defects, a new numerical tool was constructed. The model imposed an initial volume reduction defect by removing a lamina of length 2c and thickness b from an isotropic elastic media, and then applying remote compression that closes the hole. The stress pattern that resulted from the introduction of this defect was found to be characterized by compressive stress concentrations outside the defect tips, and a lowered compressive stress along the defect. Outside the defect tip, the level of stress elevation above the applied stress was constant and independent of defect length or applied stress. This stress concentration however did increase with the amount of volume removed from the defect. The conclusion is that the stress/strain distribution surrounding the LVR defect is quite different than that surrounding a mode I crack. This difference arises because the origin of stress concentrations in the two cases is different. In mode I opening/closing cracks (as long as their faces do not touch) stress concentration occurs only under application of remote load, compensating for stresses unsupported by the crack. In contrast, LVR defects do transmit load, and a stress concentration arises due to the missing volume, associated with irreversible strain.

[51] Stress concentrations at the tips of mode I cracks are responsible for their growth and evolution. It was suggested by *Fletcher and Pollard* [1981] that stress concentrations at the tips of stylolites may lead to a similar planar evolution. In the current paper we show that stress concentration at LVR defects tips is independent of LVR defect length. Thus it can be predicted that in contrast to mode I cracks, LVR defects formed by normal stress-induced processes will maintain a constant, and not accelerated, planar growth rate. In addition, because of the low stress predicted on their faces, LVR features formed by normal stress-induced processes are predicted to maintain a constant thickness, propagating in the plane only, with no further volume reduction parallel to the maximum compressive direction.

[52] Thus, looking at the morphology of known LVR features, it can also be concluded that the only feature that is probably driven by normal stress alone is compaction bands, since they show no self-similar profile in their development. However, the morphology of stylolites and spinel lenses indicates that other processes in addition to normal stresses (e.g., clay-induced dissolutions or strain energy-induced dissolution for stylolites, temperature-driven phase transformation for spinel lenses), must play a significant role in their formation, in effect offsetting the low normal stress existing on walls.

Appendix A: Model Verification

[53] Two kinds of verification were used to prove the validity of the SNM, both of them conducted on cracks. The results were obtained by using an algorithm capable of modeling both LVR and crack patterns, with the same numerical procedures (see *Katsman et al.* [2005] for details).

[54] The first verification is a comparison of the stress field obtained numerically in the vicinity of a crack tip, to that calculated according to the Griffith formulation, at constant crack length, $2c$. According to the Griffith formulation, for mode I loading, σ_{yy} at any point in the vicinity of the crack tip is [*Lawn and Wilshaw*, 1975]

$$\sigma_{yy} = \frac{K_{\mathrm{I}}}{2\pi r^{1/2}}(\cos(\theta/2)[1 + \sin(\theta/2)\sin(3\ \theta/2)]), \tag{A1}$$

where r and θ are the polar coordinates of the point with an origin at the crack tip. The stress intensity factor at the crack tip is given by

$$K_{\mathrm{I}} = M\sigma_L(\pi c)^{1/2}, \tag{A2}$$

where σ_L is the remotely applied macroscopic stress, and M is a dimensionless modification factor, arising from edge effects and given by

$$M = [L/(\pi c)\tan(\pi c/(L))]^{1/2}. \tag{A3}$$

Here L is the width of the finite plate in which the crack is embedded.

[55] Figure A1 depicts the contours for $\sigma_{yy}/(\sigma_L M)$ for both numerical and analytical solutions, calculated with $2c \cong 30$, and $L \cong 100$. It is readily seen that the obtained convergence is good.

[56] The second verification is a comparison between numerical and analytical results, of the dependence of the stress at the crack tip on the crack length. Using $\theta = 0$, and $r = 1$ in (A1) and inserting (A2), the stress in the first nonbroken unit A adjacent to the crack (Figure 6) is analytically predicted to be

$$\sigma_A = M\sigma_L\left(\frac{c}{2}\right)^{1/2}. \tag{A4a}$$

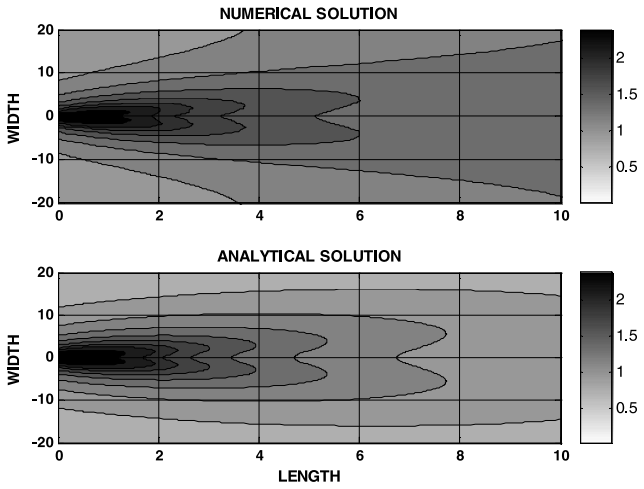

Figure A1. Comparison of numerical and analytical solutions of stress in the vicinity of a crack tip. It is readily seen that the agreement obtained is good.

As a result, σ_A is predicted to be directly proportional to the square root of the half length of the crack, or

$$\ln(\sigma_A/(M\sigma_L)) = \frac{1}{2}\ln c + \text{const.} \qquad \text{(A4b)}$$

To test modeling results against the analytical predictions of equation (A4b), σ_A was numerically calculated at unit A (Figure 6) for different crack lengths. The results are shown in Figure 7a (see curve for the crack). In Figure 7a, $\ln[\sigma_A/(\sigma_L M)]$ is plotted against $\ln c$. It is seen that for long enough cracks, $(\ln(c) \geq 2.7)$, $\ln[\sigma_A/(\sigma_L \mathrm{M})]$ is directly proportional to $\ln(c)$ so that $\ln[\sigma_A/(\sigma_L \mathrm{M})] \propto k \ln(c)$ with a coefficient $k = 1/2$, as predicted by equation (A4b). As a result, it may be concluded that the SNM simulates the stress distribution in the vicinity of a crack tip correctly, as confirmed by agreements with the Griffith theory. The algorithm used here treats both cracks and LVR defects by the same numerical procedures. Therefore, since it is proven in the case of cracks, it may be assumed to model LVR defects correctly as well.

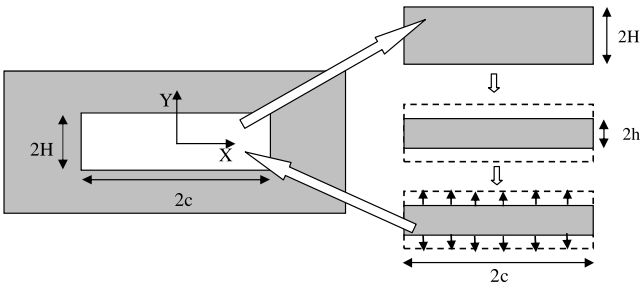

Figure B1. Localized volume reduction transformation: A rectangular region of size $H \times 2c$ is removed from an elastic body. Then an unconstrained transformation, decreasing the height $2H$ by a value b (i.e., volume reduction), took place within the rectangular region. Its length $2c$ remained unchanged. Vertical surface traction was applied in order to restore the region to its original form. Then the region was glued back into the hole in the matrix. This procedure creates a state of internal stress, which persists even in the absence of external load.

Appendix B: Eshelby Transformation Problem

[57] It was found [*Katsman et al.*, 2006] that the localized volume reduction problem is a special case of the "transformation problem" studied by *Eshelby* [1957] (Figure B1). Eshelby analytically studied a problem in which the uniformity of an elastic medium was disturbed by introducing a region within it that has changed its size or shape. Eshelby provides an alternative method to construct an LVR defect: a rectangular region of size $2H \times 2c$ was cut from the elastic body and removed from it. Then an unconstrained transformation, decreasing the vertical dimension $2H$ by value $b = 2(H - h)$ (i.e., volume reduction), took place, while defect length, $2c$, remained unchanged. Vertical surface traction was applied in order to restore the region to its original form. Then the region was "glued" back into the hole in the matrix. This procedure creates a state of internal stress, which persists even in the absence of external load. This description of an LVR lends itself to analytical stress calculations and is a special case of the *Eshelby* [1957] study on various inclusions in elastic media. Eshelby's analysis may be applicable to various types of inclusions resulting either from changed volume, as in this article, or from changes in inclusion stiffness, as in the work by *Dundurs and Markenscoff* [1989]. In fact, much progress was made using Eshelby's inhomogeneity problem to study the inclusion with zero Young's modulus and various shapes of cracks and holes.

[58] **Acknowledgments.** This research is supported by grants from BP (9749). Einat Aharonov is incumbent of the Anna and Maurice Boukstein Career Development Chair. Thanks to R. Fletcher and H. Green for suggesting the vein analogy.

References

Alvarez, W., T. Engelder, and P. A. Geiser (1978), Classification of solution cleavage in pelagic limestone, *Geology*, *6*, 263–266.

Angevine, C. L., and D. L. Turcotte (1983), Porosity reduction by pressure solution: A theoretical model for quartz arenites, *Geol. Soc. Am. Bull.*, *94*, 1129–1134.

Baud, P., E. Klein, and T.-F. Wong (2004), Compaction localization in porous sandstones: Spatial evolution of damage and acoustic emission activity, *J. Struct. Geol.*, *26*, 603–624.

Bjorkum, P. A., E. H. Oelkers, P. H. Nadeau, O. Walderhaug, and W. M. Murphy (1998), Porosity prediction in quartzose sandstones as a function of time, temperature, depth, stylolite frequency, and hydrocarbon saturation, *AAPG Bull.*, *26*, 603–624.

Budd, D. A. (2001), Permeability loss with depth in the Cenozoic carbonate platform of west-central Florida, *AAPG Bull.*, *85*(7), 1253–1272.

Budd, D. A. (2002), The relative roles of compaction and early cementation in the destruction of permeability in carbonate grainstones: A case study from the Paleogene of west-central Florida, USA, *J. Sediment. Res.*, *72*(1), 116–128.

Chaudhuri, R. A. (2003a), Eigenfunction expansion solutions for three-dimensional rigid planar inclusion problems, *Int. J. Fract.*, *121*, 95–110.

Chaudhuri, R. A. (2003b), Three-dimensional asymptotic stress fielding the vicinity of the circumference of a penny shaped discontinuity, *Int. J. Solids Struct.*, *40*(13–14), 3787–3805.

Curtin, W. A., and H. Scher (1990a), Brittle fracture in disordered materials: A spring network model, *J. Mater. Res.*, *5*(3), 535–553.

Curtin, W. A., and H. Scher (1990b), Mechanics modeling using a spring network, *J. Mater. Res.*, *5*(3), 554–562.

David, C., B. Menendez, W. Zhu, and T.-f. Wong (2001), Mechanical compaction, microstructures and permeability evolution in sandstones, *Phys. Chem. Earth A*, *26*(1–2), 45–51.

de Meer, S., and C. J. Spiers (1999), On mechanisms and kinetics of creep by intergranular pressure solution, in *Growth, Dissolution and Pattern Formation in Geosystems*, edited by B. Jamtveit and P. Meakin, pp. 345–366, Springer, New York.

Dewers, T., and P. Ortoleva (1990), A coupled reaction/transport/mechanical model for intergranular pressure solution, stylolites, and differential compaction and cementation in clean sandstones, *Geochim. Cosmochim. Acta*, *54*, 1609–1625.

Dundurs, J., and X. Markenscoff (1989), A Green's function formulation of anticracks and their interaction with load-induced singularities, *Trans. ASME*, *56*, 550–555.

Eshelby, J. D. (1957), The determination of the elastic field of an ellipsoidal inclusion, and related problems, *Proc. R. Soc. London, Ser. A*, *241*(1226), 376–396.

Fletcher, R. C., and D. D. Pollard (1981), Anticrack model for pressure solution surfaces, *Geology*, *9*, 419–424.

Fueten, F., and P.-Y. F. Robin (1992), Finite element modeling of the propagation of a pressure solution cleavage seam, *J. Struct. Geol.*, *14*(8/9), 953–962.

Gal, D., A. Nur, and E. Aharonov (1998), Stability of pressure solution surfaces, *Geophys. Res. Lett.*, *25*, 1237–1240.

Green, H. W., C. H. Scholz, T. N. Tingle, T. E. Young, and T. A. Koczynski (1992), Acoustic emission produced by anticrack faulting during the Olivine-Spinel transformation, *Geophys. Res. Lett.*, *19*(8), 789–792.

Griffith, A. A. (1920), The phenomena of rupture and flow in solids, *Philos. Trans. R. Soc. London, Ser. A*, *221*, 163–198.

Haimson, B. C. (2001), Fracture-like borehole breakouts in high porosity sandstone: Are they caused by compaction bands?, *Phys. Chem. Earth, Part A*, *26*, 15–20.

Haimson, B. C. (2003), Borehole breakouts in Berea Sandstone reveal a new fracture mechanism, *Pure Appl. Geophys.*, *160*, 813–831.

Haimson, B. C., and J. Kovachich (2003), Borehole instability in high-porosity Berea sandstone and factors affecting dimensions and shape of fracture-like breakouts, *Eng. Geol.*, *69*, 219–231.

He, D.-C. (1998), More on stress invariance conditions for the traction boundary value problem of plane linear elasticity, *Int. J. Solids Struct.*, *35*(26–27), 3519–3537.

He, W. W., A. Hajash, and D. Sparks (2002), A model for porosity evolution during creep compaction of sandstones, *Earth Planet. Sci. Lett.*, *197*(3–4), 237–244.

Issen, K. A., and J. W. Rudnicki (2000), Conditions for compaction bands in porous rock, *J. Geophys. Res.*, *105*, 21,529–21,536.

Issen, K. A., and J. W. Rudnicki (2001), Theory of compaction bands in porous rock, *Phys. Chem. Earth, Part A*, *26*(1–2), 95–100.

Karcz, Z., and C. H. Scholz (2003), The fractal geometry of some stylolites from the Calcare Massiccio Formation, Italy, *J. Struct. Geol.*, *25*(8), 1301–1316.

Katsman, R., and E. Aharonov (2006), A study of compaction bands originating from cracks, notches, and compacted defects, *J. Struct. Geol.*, in press.

Katsman, R., E. Aharonov, and H. Scher (2005), Numerical simulation of compaction bands in high-porosity sedimentary rock, *Mech. Mater.*, *37*(1), 143–162.

Katsman, R., E. Aharonov, and H. Scher (2006), Localized compaction in rocks: Eshelby's inclusion and the spring network model, *Geophys. Res. Lett.*, doi:10.1029/2005GL025628, in press.

Klaetsch, A. R., and B. C. Haimson (2002), Porosity-dependent fracture-like breakouts in St. Peter sandstone, in *Mining and Tunneling Innovation and Opportunity*, edited by R. Hammah et al., 1365–1371, Univ. of Toronto Press, Toronto, Ont., Canada.

Koehn, D., J. Arnold, B. Jamtveit, and A. Malthe-Soressen (2003), Instabilities in stress corrosion and the transition to brittle failure, *Am. J. Sci.*, *303*, 956–971.

Lawn, B. R., and T. R. Wilshaw (1975), *Fracture of Brittle Solids*, Cambridge Univ. Press, New York.

Lehner, F. K. (1995), A model for intergranular pressure solution in open systems, *Tectonophysics*, *245*, 153–170.

Markenscoff, X. (1993), On the Dundurs correspondence between cavities and rigid inclusions, *J. Appl. Mech.*, *60*, 260–264.

Markenscoff, X., and M. Paukshto (1995), On the Dundurs correspondence between cavities and rigid inclusions, *Int. J. Solids Struct.*, *32*(3–4), 431–438.

Mollema, P. N., and M. A. Antonellini (1996), Compaction bands: A structural analog for anti-mode I crack in aeolian sandstone, *Tectonophysics*, *267*, 209–228.

Niemeijer, A., C. J. Spiers, and B. Bos (2002), Compaction creep of quartz sand at 400–600°C: Experimental evidence for dissolution-controlled pressure solution, *Earth Planet. Sci. Lett.*, *195*(3–4), 261–275.

Olsson, W. A. (1999), Theoretical and experimental investigation of compaction bands in porous rock, *J. Geophys. Res.*, *104*, 7219–7228.

Olsson, W. A. (2001), Quasistatic propagation of compaction fronts in porous rock, *Mech. Mater.*, *33*, 659–668.

Olsson, W. A., and D. J. Holcomb (2000), Compaction localization in porous rock, *Geophys. Res. Lett.*, *27*(21), 3537–3540.

Paterson, M. S. (1973), Nonhydrostatic thermodynamics and its geological applications, *Rev. Geophys.*, *11*(2), 355–389.

Ramm, M. (1992), Porosity depth trends in reservoir sandstones - theoretical-models related to Jurassic sandstones offshore Norway, *Mar. Pet. Geol.*, *9*(5), 553–567.

Ramos, J. R. A. (2000), Stylolites: Measurement of rock loss, *Rev. Brasil. Geoci.*, *30*(3), 432–435.

Renard, F., P. Ortoleva, and J. P. Gratier (1997), Pressure solution in sandstones: Influence of clays and dependence on temperature and stress, *Tectonophysics*, *280*(3–4), 257–266.

Renard, F., A. Park, P. Ortoleva, and J.P. Gratier (1999), An integrated model for transitional pressure solution in sandstones, *Tectonophysics*, *312*(2–4), 97–115.

Renard, F., J. Schmittbuhl, J. Gratier, P. Meakin, and E. Merino (2004), Three-dimensional roughness of stylolites in limestones, *J. Geophys. Res.*, *109*, B03209, doi:10.1029/2003JB002555.

Revil, A., D. Grauls, and O. Brévart (2002), Mechanical compaction of sand/clay mixtures, *J. Geophys. Res.*, *107*(B11), 2293, doi:10.1029/2001JB000318.

Riggs, E. M., and H. W. Green II (2005), A new class of microstructures which lead to transformation-induced faulting in magnesium germanate, *J. Geophys. Res.*, *110*, B03202, doi:10.1029/2004JB003391.

Rudnicki, J. W., and W. A. Olsson (1998), Reexamination of fault angles predicted by shear localization theory, *Int. J. Rock Mech. Min. Sci.*, *35*(4/5), 512–513.

Rutter, E. H. (1976), The kinetics of rock deformation by pressure solution, *Philos. Trans. R. Soc. London, Ser. A*, *283*, 203–220.

Schlangen, E., and E. J. Garboczi (1996), New method for simulating fracture using an elastically uniform random geometry lattice, *Int. J. Eng. Sci.*, *34*(10), 1131–1144.

Schlangen, E., and E. J. Garboczi (1997), Fracture simulations of concrete using lattice models: Computational aspects, *Engineering Fracture Mechanics*, *57*(2/3), 319–332.

Scholz, C. H. (2000), *The Mechanics of Earthquakes and Faulting*, Cambridge Univ. Press, New York.

Stockdale, P. B. (1922), Stylolites: Their nature and origin, *Indiana Univ. Studies*, *9*, 1–97.

Thorpe, M. F., and I. Jasiuk (1992), New results in the theory of elasticity for 2-dimensional composites, *Proc. R. Soc. London, Ser. A*, *438*, 531–544.

Vajdova, V., and T. Wong (2003), Incremental propagation of discrete compaction bands: Acoustic emission and microstructural observations on circumferentially notched samples of Bentheim, *Geophys. Res. Lett.*, *30*(14), 1775, doi:10.1029/2003GL017750.

Vajdova, V., T.-F. Wong, D. E. Farell, K. A. Issen, and V. Challa (2003), Experimental observation and numerical simulation of initiation and propagation of compaction bands in a sandstone, paper presented at ASCE Engineering Mechanics Conference, Am. Soc. of Civ. Eng., Seattle, Wash., 16–18 July.

Vajdova, V., P. Baud, and T. Wong (2004), Permeability evolution during localized deformation in Bentheim sandstone, *J. Geophys. Res.*, *109*, B10406, doi:10.1029/2003JB002942.

Vanucchi, P. (2001), Monitoring paleo-fluid through vein microstructures, *J. Geodyn.*, *32*, 567–581.

Walderhaug, O., and P. A. Bjorkum (2003), The effect of stylolite spacing on quartz cementation in the lower Jurassic Sto Formation, southern Barents Sea, *J. Sediment. Res.*, *73*(2), 146–156.

Weyl, P. K. (1959), Pressure-solution and the force of crystallization: A phenomenological theory, *J. Geophys. Res.*, *64*, 2001–2025.

Wong, T.-f., C. David, and W. Zhu (1997), The transition from brittle faulting to cataclastic flow in porous sandstone: Mechanical deformation, *J. Geophys. Res.*, *102*, 3009–3025.

Wong, T.-f., P. Baud, and E. Klein (2001), Localized failure modes in compactant porous rock, *Geophys. Res. Lett.*, *28*, 2521–2524.

E. Aharonov, R. Katsman, and H. Scher, Weizmann Institute of Science, 76100 Rehovot, Israel. (regina.katsman@weizmann.ac.il)